Evaluation of Cell Mismatch in Pre-Exposure Photovoltaic Modules Using Electroluminescence Imaging

Janis J. B. Galdino[1], João V. F. F. de Medeiros[1], Olga de C. Vilela[1], Emerson T. A. Gomes[1] and Naum Fraidenraich[1]

[1] Center for Renewable Energy, Federal University of Pernambuco, Recife (Brazil)

Abstract

The objective of this study is to analyze the impact of cell mismatch on the maximum power output in a case study involving seven PV modules from the same manufacturing batch. Since the cells are connected in series, module assembly is performed using cells from the same performance bin to minimize mismatch losses and the manufacturer specifies a batch power tolerance. However, once a PV module is encapsulated, measuring the electrical behavior of individual cells becomes a non-trivial task. In this work, cell mismatch was evaluated by correlating electroluminescence (EL) image pixel intensity with current-voltage (I-V) curve measurements. With the EL images, a normalized brightness matrix for each module was created. The results showed that 5 from the 7 modules presented underperformance (fake power) related to cell mismatch. These findings suggest that low and highly variable cell brightness—potentially resulting from inadequate cell sorting during module assembly—can be associated with underrated power.

Keywords: cell mismatch, underperformance PV module, electroluminescence, pre-exposure PV module, fake power.

1. Introduction

One of the most common causes of power loss in photovoltaic (PV) modules is mismatch between their cells. Since the cells are connected in series, differences in their electrical characteristics can limit the overall power output of the module, which depends on the combined current and voltage behavior of all cells. As a result, PV modules are manufactured using cells with closely matched electrical properties to maximize performance. To achieve this, PV cells are sorted during production based on their electrical performance, typically indicated by efficiency evaluated through current-voltage (I-V) curve measurements (Wilson et al., 2006). Other sorting criteria may also be used, such as maximum power output, current at a specified voltage, current at the maximum power point, or combinations of these indicators (Sabater et al. 2018; Forniés et al. 2013). Module assembly is then performed using cells from the same performance bin to minimize mismatch losses and the manufacturer specifies a batch power tolerance. However, recent advances in cell manufacturing—such as larger and thinner wafers, novel busbar designs (including busbarless cells), and the adoption of half or quarter-cell formats—introduce technical challenges to I-V curve measurements, requiring adaptations in contacting methods (Buratti et al., 2021). Additionally, the increasing use of bifacial solar cells adds further complexity to the sorting process, as cell performance is influenced by both front and rear illumination characteristics (Sabater et al. 2018).

In the solar industry, accurately characterizing the I–V behavior of individual cells within an encapsulated PV module is valuable for assessing the impact of cell mismatch on module power output. However, once a PV module is encapsulated, measuring the electrical behavior of individual cells becomes a non-trivial task. Non-destructive alternatives include analyzing I-V curves under partial shading or using the Suns-Voc method, which involves measuring the open-circuit voltage (Voc) under varying illumination (Blakesley et al., 2020; Wilson et al., 2006). A more practical and widely used technique for identifying cell mismatch within a PV module is electroluminescence (EL) imaging. This method captures the light emitted by solar cells when electrical current is injected in forward bias. The intensity of light observed in EL images correlates with cell performance, and the technique is commonly employed to detect defects. When combined with deep learning

10.18086/swc.2025.03.28 Available at http://proceedings.ises.org

and machine learning algorithms, EL imaging becomes a powerful tool not only for defect detection and diagnosis but also for quantitatively estimating the electrical performance of individual cells within a module (Buratti et al., 2021; Rajput et al., 2018).

In this context, the objective of this study is to analyze the impact of cell mismatch on the maximum power output in a case study involving seven PV modules from the same manufacturing batch, by correlating electroluminescence (EL) image pixel intensity with I–V curve measurements.

2. Methodology

Seven photovoltaic (PV) modules from the same production batch of a manufacturer were evaluated prior to exposure. According to the datasheet, the rated power of each module is 450 W. The modules use monocrystalline silicon (m-Si) PERC bifacial technology with 144 half-cells. The power tolerance informed by the manufacturer is 0~+5 W. Acquired in 2022, they were subjected to I-V curve measurements and electroluminescence (EL) testing prior to exposure.

The I-V curves under standard test conditions (STC) were obtained using the Argus SMTL-V21.3A+ flash solar simulator, shown in Figure 1. For each module, 3 I-V curves were taken.

Figure 1: Solar simulator Argus SMTL-V21.3A+. Source: https://www.argussolar.net/prolist01s5/72-362.html

The I–V curve of a PV module can be parameterized using the one-diode model, as shown in Eq. (1), which represents a photovoltaic cell as a current source connected to a diode with parasitic resistances (series and shunt) (Green, 1981).

$$I = I_L - I_0\left(e^{\frac{V+IR_S}{mV_T}} - 1\right) - \frac{V-IR_S}{R_{SH}} \qquad \text{(eq. 1)}$$

Where V_T is the module thermal voltage given by Eq. (2).

$$V_T = n_s\frac{kq}{T} \qquad \text{(eq. 2)}$$

Where n_S is the number of cells connected in series in the module, k is the Boltzmann constant, q is the elementary charge and T is the mean module cell temperature.

To fit the I–V curve data obtained from the solar simulator, the one-diode model equation was rearranged into Eq. (3) to incorporate the Lambert W function, as described by Cubas *et al.* (2014) and Jain and Kapoor (2005). The parameters of series resistance (R_S), shunt resistance (R_{SH}), diode ideality factor (m), reverse saturation current (I_0) and photogenerated current (I_L) were determined through a non-linear fitting procedure based on the Levenberg–Marquardt least-squares algorithm, implemented using the *SciPy* library in Python 3.12 (Vugrin et al., 2007).

The one-diode model parameter extraction was conducted to assess the semiconductor quality of the PV modules and to analyze its influence on their electrical characteristics.

$$I = r + \frac{1}{c} W^{-1}\left(\frac{ce^{-cr}}{a_0}\right) \quad \text{(eq. 3)}$$

$$where\ r = (I_L + I_0)\left(\frac{R_{SH}}{R_S + R_{SH}}\right) - \frac{V}{R_S + R_{SH}} \quad \text{(eq. 4)}$$

$$a_0 = \left(-\frac{1}{I_0}\right)\left(\frac{1}{e^{\frac{V}{mV_T}}}\right)^{\frac{(R_S + R_{SH})}{R_{SH}}} \quad \text{(eq. 5)}$$

$$c = -\frac{R_S}{mV_T} \quad \text{(eq. 6)}$$

EL images were captured with a Nikon D5600 camera equipped with a silicon-based Complementary Metal-Oxide-Semiconductor (CMOS) sensor and appropriate optical filters. During the EL test, each module was forward-biased using a power supply to inject electrical current approximately equal to the short-circuit current (I_{sc}).

Post-processing of the EL images was performed using Python-based algorithms and involved the following steps: i) detection of module boundaries; ii) reprojection into a flat, rectangular image to correct for tilt and perspective distortion; iii) conversion of the RGB image to grayscale, assigning each pixel a value between 0 (black) and 255 (white) using the OpenCV library; iv) division of the module into a grid of cells; v) calculation of the mean pixel value (brightness) for each cell; and vi) normalization of cell brightness values relative to the brightest cell in the module. As a result, the algorithm generated a normalized brightness matrix for each module.

3. Results

Table 1 presents the maximum power at STC (P_{max}), open-circuit voltage (V_{OC}), short-circuit current (I_{SC}), current at the Pmax (I_{MP}), and voltage at Pmax (V_{MP}) obtained from the I-V curve measurements for all seven PV modules, labeled M1 through M7. With exception of M4 and M7, all the modules exhibit underperformance that exceeds the power tolerance informed by the manufacturer. Notably, the module M5 shows a deviation greater than 2% compared to the P_{max} specified in the datasheet. Regarding the other electrical parameters, the differences among the modules appear to be minimal. However, modules M4 and M7 consistently exhibit the highest values.

Table 1: Electrical parameters from the I-V curve measurements for the PV modules under study.

	M1	**M2**	**M3**	**M4**	**M5**	**M6**	**M7**
P_{max} (W)	448.67 ± 0.01	445.67 ± 0.02	443.88 ± 1.34	449.87 ± 0.14	439.41 ± 0.10	444.42 ± 0.10	450.05 ± 0.02
V_{oc} (V)	49.28± 0.01	49.18± 0.01	49.11± 0.12	49.37± 0.01	48.94± 0.01	49.11± 0.01	49.44± 0.01
I_{cc} (A)	11.32± 0.01	11.29± 0.01	11.23± 0.01	11.34± 0.01	11.26± 0.01	11.24± 0.01	11.36± 0.01
I_{mp} (A)	10.65± 0.01	10.62± 0.01	10.63± 0.02	10.69± 0.01	10.60± 0.02	10.60± 0.01	10.68± 0.02
V_{mp} (V)	42.14± 0.03	41.96± 0.05	41.77± 0.19	42.10± 0.02	41.45± 0.08	41.94± 0.02	42.12± 0.08

Figure 2 exhibits the EL image, along with the corresponding heatmap generated from its normalized cell brightness, for the M3, M5 and M7 modules. A significant non-uniformity in the light intensity emitted by the module's cells is observed in the EL image for the M3 module. In this case, the darkest cell emits only approximately 50% of the light intensity of the brightest cell. Similar results were found for the M1, M2, and M6 modules. The module M7 displays the highest and most uniform light intensity emission, which is consistent with its superior performance among the analyzed samples. That is also the case for M4 module. In contrast, visually, the module M5 exhibits a large number of cells with low light intensity, although the distribution of light emission across its cell is more uniform than the modules M1, M2, M3 and M6.

The normalized brightness variance for the seven modules is illustrated by the boxplots in Figure 3-a. Modules M4 and M7 exhibit the highest median brightness values and the lowest dispersion among all samples. Notably, these are the only two modules whose P_{max} falls within the power tolerance specified by the manufacturer. In contrast, the modules M3 and M6 demonstrate not only lower median brightness but also a significantly higher variation in brightness among their cells. Although, the most underperforming module, M5, presents a low brightness variation and seems to be manufactured with a set of low brightness cell. Figure 3-b presents the number of cells with normalized brightness below 75%, showing that the most underperforming modules correspond to those with the highest number of low-brightness cells. These results suggest that low and highly variable cell brightness can be associated with unrated power potentially caused by an inadequate cell sorting during module assembly.

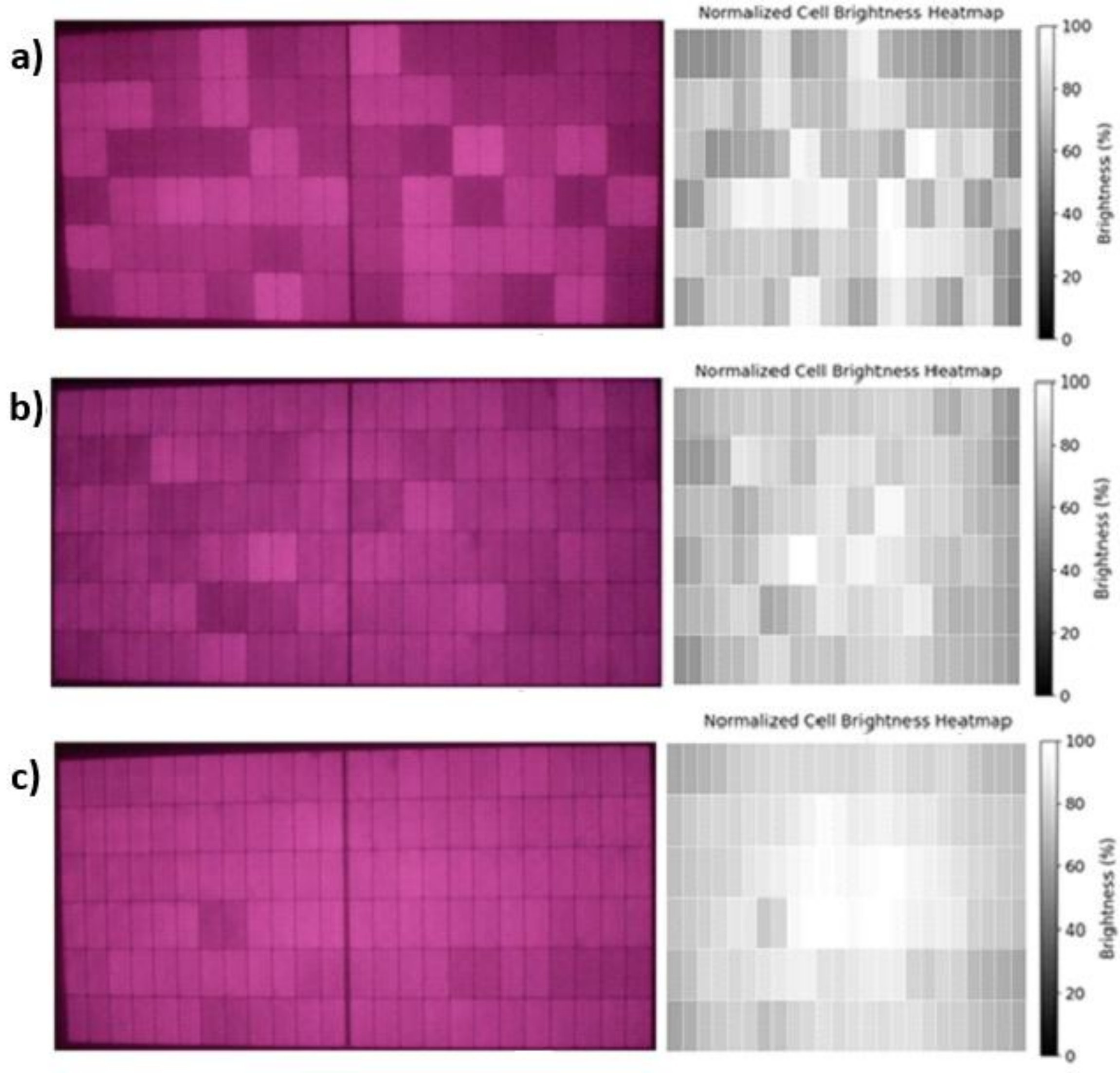

Figure 2: EL image and normalized cell brightness heatmap for the modules: a) M3, b) M5, and c) M7.

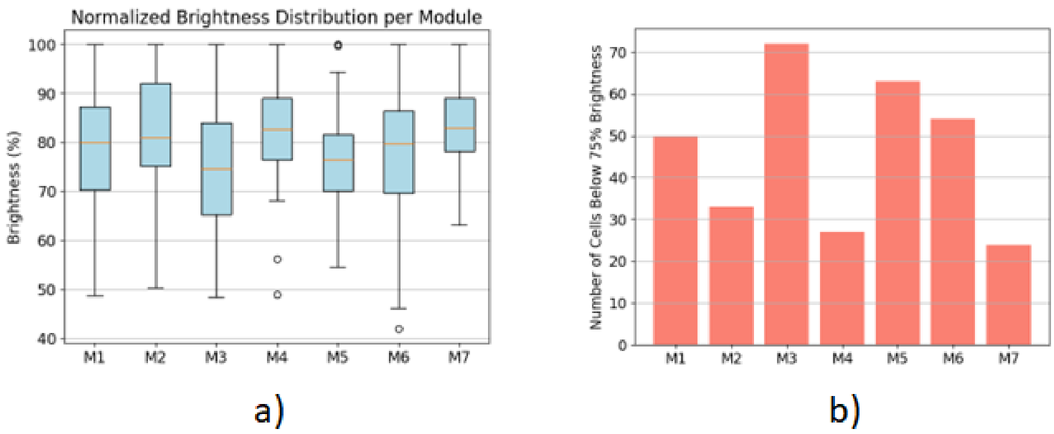

Figure 3: a) Boxplot of the normalized brightness of the modules; b) number of cells with normalized brightness below 75%.

The I-V curves of the modules M6 and M7 are presented in Figure 4, illustrating how the one-diode Lambert fitting method accurately reproduces the measured I–V data. Across all seven modules (21 I-V curves in total), the mean root mean square error (RMSE) for the simulated current was 0.04 A.

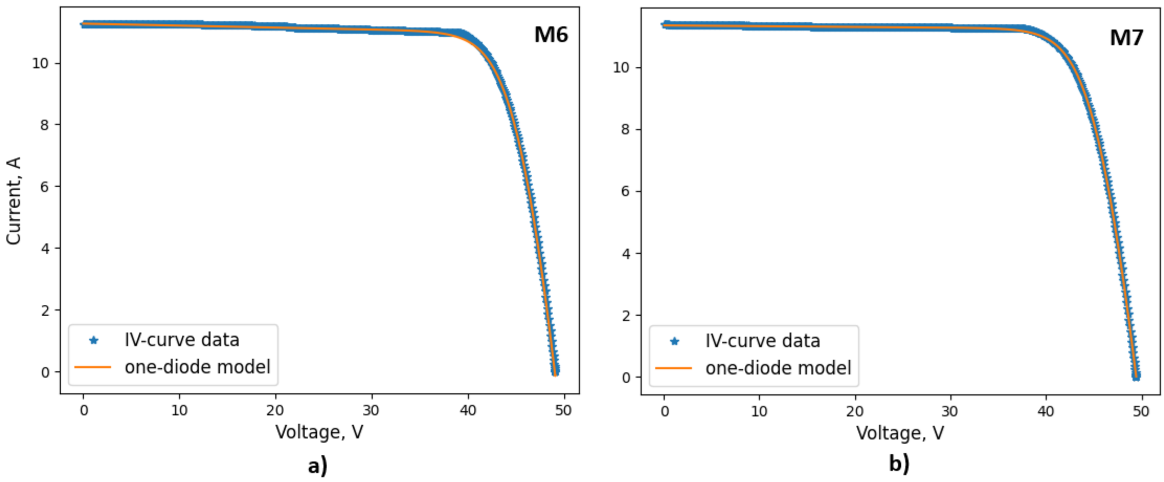

Figure 4: IV-curve data and one-diode model fitting for the modules: a) M6, and b) M7.

Table 2 exhibits the parameters of R_S, R_{SH}, m, I_0 and I_L obtained for each module. It can be noted that with exception of R_{SH}, all the others parameters present similar values. Modules M1, M2, and M6 show the lowest R_{SH} values, and all of them demonstrate underperformance, as shown in Table 1. However, the higher R_{SH} values observed for M3 and M5 indicate that the relationship between this parameter and inadequate cell sorting requires further investigation.

Table 2: One-diode model parameters for all modules under study.

One-diode parameters	M1	M2	M3	M4	M5	M6	M7
R_S (Ω)	0.21	0.21	0.24	0.23	0.26	0.21	0.23
R_{SH} (Ω)	188.36	174.45	706.22	559.75	426.62	159.97	424.58
m	1.048	1.046	1.045	1.05	1.041	1.044	1.051
I_0 (A)	1.01E-10	9.95E-11	1.01E-10	1.03E-10	1.01E-10	1.02E-10	1.02E-10
I_L (A)	11.345	11.31	11.202	11.32	11.246	11.275	11.34

4. Conclusion

The analysis of seven PV modules from the same manufacturing batch demonstrated a clear correlation between cell mismatch, as revealed by electroluminescence imaging, and module underperformance determined through I–V curve measurements. Among the analyzed samples, only modules M4 and M7 exhibited power outputs within the tolerance range specified by the manufacturer. These two modules also showed the highest and most uniform EL brightness, confirming the relationship between uniform light emission and electrical behavior.

In contrast, modules presenting significant non-uniformity in EL brightness—particularly M1, M2, M3, M5, and M6—displayed lower maximum power values and higher deviations from the datasheet specifications (fake power). The analysis of normalized brightness variance reinforced this observation, as modules with greater brightness dispersion and a higher number of low-brightness cells corresponded to those with the largest power losses.

Overall, the results indicate that inadequate cell sorting during module assembly can lead to cell mismatch and, consequently, to unrated power output. EL imaging combined with electrical characterization thus proves to be an effective, non-destructive diagnostic tool for assessing module uniformity and detecting mismatch-related losses prior to field exposure.

5. Acknowledgments

The authors thank the Fundação de Amparo à Ciência e Tecnologia de Pernambuco (Facepe. Grant Number APQ-2274-3.14/24). This work is part of the Instituto Pernambucano de Ciência. Tecnologia e Inovação (IPECTI) em Energias Renováveis e Descarbonização (Rede Zero C).

6. References

Blakesley. J. C.. Castro. F. A.. Koutsourakis. G.. Laudani. A.. Lozito. G. M.. and Fulginei. F. R. 2020. “Towards non-destructive individual cell IV characteristic curve extraction from photovoltaic module measurements”. Solar Energy. 202. pp. 342-357.

Buratti. Y.. Sowmya. A.. Evans. R.. Trupke. T.. and Hameiri. Z. 2022. “Half and full solar cell efficiency binning by deep learning on electroluminescence images”. Progress in Photovoltaics: Research and Applications. 30(3). pp. 276-287.

Cubas. J.. Pindado. S.. & De Manuel. C. 2014. Explicit expressions for solar panel equivalent circuit parameters based on analytical formulation and the Lambert W-function. Energies. 7(7). 4098-4115.

Forniés. E.. Naranjo. F.. Mazo. M.. and Ruiz. F. 2013. The influence of mismatch of solar cells on relative power loss of photovoltaic modules. Solar Energy. 97. pp. 39-47.

Green. M. A. 1981. Solar cells: operating principles. technology. and system applications. Prentice Hall. pp. 13-37.

Jain. A.. & Kapoor. A. 2005. A new approach to study organic solar cell using Lambert W-function. Solar energy materials and solar cells. 86(2). 197-205.

Rajput. A. S.. Ho. J. W.. Zhang. Y.. Nalluri. S.. and Aberle. A. G. 2018. “Quantitative estimation of electrical performance parameters of individual solar cells in silicon photovoltaic modules using electroluminescence imaging”. Solar Energy. 173. pp. 201-208.

Sabater. A. A.. Wöhrle. N.. Greulich. J. M.. Rein. S.. and Ramspeck. K. 2018. “Impact of bifacial illumination and sorting criteria of bifacial solar cells on module power”. In AIP Conference Proceedings. 1999(1).

Wilson. K.. De Ceuster. D.. and Sinton. R. A. 2006. “Measuring the effect of cell mismatch on module output”. In 2006 IEEE 4th World Conference on Photovoltaic Energy Conference. 1. pp. 916-91.

Vugrin. K. W.. Swiler. L. P.. Roberts. R. M.. Stucky-Mack. N. J.. & Sullivan. S. P. (2007). Confidence region estimation techniques for nonlinear regression in groundwater flow: Three case studies. Water Resources Research. 43(3).